Co-Aromatization of Furan and Methanol over ZSM-5 - A Pathway to Bio-Aromatics

Uslamin, Evgeny A.; Kosinov, Nikolay; Filonenko, Georgy A.; Mezari, Brahim; Pidko, Evgeny; Hensen, Emiel J.M.

DOI
10.1021/acscatal.9b02259

Publication date
2019

Document Version
Accepted author manuscript

Published in
ACS Catalysis

Co-aromatization of Furan and Methanol over ZSM-5 – A Pathway to Bio-Aromatics

Evgeny A. Uslamin,[a] Nikolay Kosinov,[a] Georgy A. Filonenko,[b] Brahim Mezari,[a] Evgeny Pidko,*[b] and Emiel J.M. Hensen*[a]*

[a] Inorganic Materials & Catalysis group, Eindhoven University of Technology, PO Box 513, 5600 MB Eindhoven, The Netherlands

[b] Inorganic Systems Engineering group, Delft University of Technology, 2629 HZ Delft, The Netherlands

E-mail: n.a.kosinov@tue.nl (NK) e.a.pidko@tudelft.nl (EP); e.j.m.hensen@tue.nl (EJMH)

ABSTRACT Aromatization of furan and substituted furans over zeolite catalysts is a promising reaction to convert cellulose-derived compounds into valuable aromatic hydrocarbons and light olefins. A lack of understanding of the reaction mechanism however hinders further development of this process. Here, we propose the reaction mechanism, underlying the chemistry of furan and methanol co-aromatization over HZSM-5 zeolite catalyst. Applying ^{13}C isotope labelling in a combination with NMR spectroscopy and high temporal resolution GC-MS analysis, we demonstrate that aromatization of furan and methanol are not mechanistically separated and can be described within the Dual-Cycle hydrocarbon pool mechanism. Co-feeding furan with methanol leads to a significant enhancement of light aromatics selectivity and increased catalyst lifetime.

KEYWORDS Aromatics; biomass; furan, methanol-to-aromatics; zeolite.

Introduction

Replacing fossil-based feedstock by renewable alternatives remains a substantial challenge for the chemical industry. Aromatic compounds, which are the basic building blocks for the production of a wide range of polymers, solvents and fine chemicals, are currently obtained exclusively from petroleum feedstock. As lignocellulosic biomass is considered one of the main sources of renewable carbon, chemical conversion routes to bio-based aromatics are highly desirable. Valorization of biomass into chemical commodities requires several separation steps and chemical conversion steps, including depolymerization and oxygen removal. A common approach is to convert biomass into platform molecules from which a wider range of chemical applications can be targeted.[1–3] One of promising methods involves depolymerization of cellulose into glucose followed by its isomerization and dehydration to obtain furanic platform molecules. Furanics can be converted to aromatics at high temperature in the presence of zeolite catalysts.[4,5] Typically, shape-selective MFI-type (ZSM-5) zeolite is used as catalyst for aromatization processes, because its optimal pore size leads to high BTX selectivity.[6,7] Besides, it has been shown that furan can serve as a representative model compound for catalytic fast pyrolysis (CFP) of raw woody biomass.[5,8] A major drawback of the aromatization of furanics is the rapid deactivation of the zeolite catalyst and the relatively low aromatic selectivity.[9,10] Diels-Alder (DA) chemistry is commonly thought to form the mechanistic basis for the conversion of furanics to aromatics over zeolites. Furanics and reaction intermediates formed via deoxygenation during pyrolysis may act simultaneously as dienes and dienophiles.[5,11,12] Based on this idea, ethylene and propylene co-feeding during pyrolytic upgrading has been explored. In such studies, it has been observed that the selectivity to benzene, toluene and xylenes (BTX) is improved when olefins are added to the feed.[11,13–15] In practice, such olefins are however too expensive to facilitate the production of

aromatics via this route. Recently, it has been suggested that methanol co-feeding can also enhance the BTX selectivity in the zeolite-catalyzed upgrading processes, presumably because methanol is rapidly converted to olefins on the same zeolite catalysts.[16,17] In this work, we study the effect of methanol addition on the aromatization of furan over zeolite catalysts. By applying isotopic labelling and NMR spectroscopy, we elucidate the different mechanistic pathways that underlie the co-aromatization of furan and methanol. A major insight is that this process does not involve DA chemistry and is predominantly based on the hydrocarbon pool mechanism. Based on our findings, we optimized this process, which may link the renewable energy storage via carbon dioxide hydrogenation to liquid methanol with renewable biomass for the manufacture of important chemical intermediates.[18–20]

1. Experimental Procedures

1.1. Catalyst characterization

The ammonium form of zeolite ZSM-5 with Si/Al ratio of 40 (obtained from Alfa Aesar) was calcined at 550 °C for 5 hours in static air (heating rate 5 °C/min) to obtain the proton form HZSM-5.

The chemical composition (Si/Al ratio) of zeolite was determined by elemental analysis using ICP-OES. A Spectro CIROS CCD ICP optical emission spectrometer with axial plasma viewing was used for these measurements. Prior to analysis, the zeolite samples were dissolved in a 1:1:1 mixture by weight of HF (40 %), HNO_3 (60 %), and H_2O.

The fraction of extra-framework Al was assessed by ^{27}Al magic angle spinning nuclear magnetic resonance (MAS NMR) spectroscopy. The measurements were carried out using a 11.7 T Bruker DMX500 NMR spectrometer with a 2.5 mm MAS probe head spinning at 25 kHz. The sample was hydrated prior to NMR measurements. ^{27}Al NMR spectra were recorded with a single pulse sequence with a 18° pulse, duration of 1 μs and interscan delay of 1 s.

The acidic properties were determined by IR spectroscopy of adsorbed pyridine. Spectra were taken in the 4000–1000 cm^{-1} range using a Bruker Vertex 70v Fourier-transform infrared spectrometer. Samples were pressed into self-supporting wafers (10−15 mg, diameter 1.3 cm) and placed in an environmental cell. The wafers were first pre-treated in O_2:N_2 (1:4 vol. ratio) flow at 550 °C (heating rate 5 °C/min) to remove contaminants followed by cooling to 150 °C under dynamic vacuum ($p < 10^{-5}$ mbar). Pre-treated wafers were then exposed to excess pyridine vapor. After evacuation, IR spectra were recorded at different temperatures (150–450 °C) under vacuum.

For the quantification of Brønsted and Lewis acid sites, integral molar extinction coefficients (IMEC) of 0.73 cm/mol and 1.11 cm/mol, respectively, were used.[21,22]

Textural properties of the zeolites were determined from Ar physisorption isotherms, which were recorded at 87.3 K using a Micromeritics ASAP-2020 apparatus. The sample was outgassed at 450 °C prior to physisorption. The microporous volume was determined by the *t*-plot method using a thickness range from 3.5 to 4.5 Å.

1.2. Catalytic activity measurements

Catalytic activity measurements were carried out in a tubular quartz fixed-bed downstream reactor (i.d. = 4 mm, l = 20 cm). In a typical experiment, 0.5 g catalyst (sieve fraction of 250–500 μm) was held in between two quartz wool plugs. Prior to the measurements, zeolite was pre-treated under O_2:He (1:4 vol. ratio) flow at 550 °C (heating rate 5 °C/min) to remove water and any possible organic contaminants and then cooled down to the reaction temperature. Calibrated thermal mass-flow controllers (Brooks) were used to feed carrier gases to the saturators and to the reactor. Furan (Sigma Aldrich, ≥ 99 %), 2.5-dimethylfuran (2.5-dMF, Sigma Aldrich, 99 %) and methanol (VWR chemicals, 99,9%) were introduced in the feed by leading a gas flow through thermostated saturators. For isotope labelling experiments ^{13}C ethylene (Eurisotop, 98 %, 99 % ^{13}C) and ^{13}C methanol (Cambridge Isotope Laboratories, 98 %, 99 % ^{13}C) were used.

Reaction products were analyzed with online mass spectrometry (Pfeiffer Omnistar GSD 301 T3 MS) and gas chromatography (Trace GC 1300, Thermo) instruments, placed consecutively downstream the reactor. A TCD detector equipped with an RT-Q-Bond column (length 20 m; i.d. 0.32 mm; d.f. 10 μm) was used to analyze the light fraction of the reaction products including water, CO_x andC_1 – C_4 hydrocarbons. Aromatic products were analyzed with an FID detector

coupled with Rxi-5Sil MS column (length 30 m; i.d. 0.32 mm; d.f. 0.25 μm). For qualitative analysis and identification of individual compounds, the reaction products were collected in a cold trap (cooled with liquid nitrogen) and then analyzed with a GC-MS instrument (Shimadzu MS GCMS-QP 5050a). A mixture of GC standards was used to confirm the assignment of the main components. The reaction selectivity, conversion and yield were calculated as follows:

$$\text{(I)} \qquad x_i(t) = \frac{n_i^{out}}{n_i^{in}};$$

$$\text{(II)} \qquad s_k(t) = \frac{n_k^{out}}{n_i^{in} - n_i^{out}} * \left|\frac{\mu_i}{\mu_k}\right|;$$

$$\text{(III)} \qquad X_\Sigma(C_{based}) = \sum_i \mu_i * \int_0^t (n_i^{in} - n_i^{out})dt;$$

$$\text{(IV)} \qquad S_k = \frac{\mu_k * \int_0^t n_k^{out} dt}{X_i};$$

$$\text{(V)} \qquad Y_k = \mu_k * \int_0^t n_k^{out} dt = S_k * X_i,$$

where (I) – conversion at time t; (II) – carbon based selectivity to a product k at time t where n_j – concentration of the product k and μ_j – number of carbon atoms in the product k; (III) – overall carbon-based conversion at time t; (IV) – overall carbon-based selectivity to a product k; (V) – overall carbon-based yield of a product k. Cumulative parameters were calculated up until time t such as that x(t) = 75 %.

NMR spectra of the reaction products were measured on Bruker 400 Avance II and Agilent 400-MR DD2 spectrometers. All measurements were performed using identical concentrations and sample collection times to ensure adequate comparison between reaction mixtures, produced with ^{13}C labelled and non-labelled ethylene and methanol substrates. Samples were prepared by diluting the collected reaction mixture with 1 mL $CDCl_3$, which provided nearly identical ^{1}H spectra for natural and ^{13}C-enriched mixtures. The connectivity of ^{13}C atoms in the reaction products was studied using ^{13}C-^{13}C homonuclear correlation NMR spectroscopy (Incredible

Natural Abundance DoublE QUAntum Transfer Experiment, INADEQUATE). In all cases, non-enriched samples did not produce detectible INADEQUATE signal. The acquisition time of an INADEQUATE experiment for ^{13}C methanol sample was shortened to 64 increments (64 scans each) to ensure absence of interference from naturally abundant ^{13}C atoms.

1.3. Coke characterization

In situ IR spectroscopy was used to follow the deposited coke using a Bruker Vertex 70v Fourier-transform infrared spectrometer. For this purpose, a zeolite sample was pre-treated following the same procedure as described above. Then the chamber was evacuated under dynamic vacuum ($p < 10^{-5}$ mbar) and cooled to 450 °C. Gaseous furan, methanol and furan-methanol mixture were supplied to the chamber using a 1 ml sample loop connected to a thermostated saturator through which He was flown. IR spectra were recorded in the 4000−1000 cm^{-1} range.

Thermogravimetric analysis (TGA) of spent catalysts was measured with a Mettler Toledo TGA/DSC 1 instrument. An amount of ~15 mg of used catalyst was placed in an alumina crucible and then heated up to 700 °C at a rate of 5 °C/min in O_2:He (20:40) 60 ml/min flow.

Solid state MAS NMR spectra were measured using 11.7 Tesla Bruker DMX500 NMR spectrometer, operating at 500 MHz and 125 MHz for ^{1}H and ^{13}C respectively. The experiments were performed using a Bruker Triple Channel 4 mm MAS probe head spinning at rates between 8 and 10 kHz. Quantitative ^{13}C direct excitation (DE) MAS NMR spectra were measured with a high power proton decoupling Hahn-echo pulse sequence p1-τ1-p2-τ2-aq with a 90° pulse p1=5 μs and a 180º pulse p2=10 μs with an interscan delay of 20 s. One dimensional $^{13}C\{^{1}H\}$ cross polarization (CP) and two-dimensional ^{1}H-$^{13}C\{^{1}H\}$ HETCOR (Heteronuclear Correlation) MAS NMR spectra were recorded with a ramped contact pulse of 3 ms and an inerscan delay of 3 s. During the acquisition the ^{1}H heteronuclear decoupling was applied using the spinal-64 pulse

scheme. ^{1}H shifts were calibrated using tetramethylsilane (TMS). Solid adamantane was used for ^{13}C NMR shift calibrations.

Results and Discussion

The proton form of ZSM-5 zeolite (Si/Al 40) was used for all experiments. The material was thoroughly characterized for its physico-chemical properties (see *Table S1*). Catalytic tests were carried out in a fixed-bed quartz reactor coupled with on-line gas chromatography. Other experimental details can be found in the *Supporting Information*. The catalytic results show that aromatization of furan yields a mixture of light hydrocarbons (CH_4, C_2 – C_4 compounds), BTX and other substituted benzenes (*e.g.* ethylmethylbenzenes, trimethylbenzenes), heavier bicyclic aromatic compounds (indanes, indenes, naphthalenes) as well as water and CO_x (*Figure 1*). The numerical data of these tests are collected in *Table S2*.

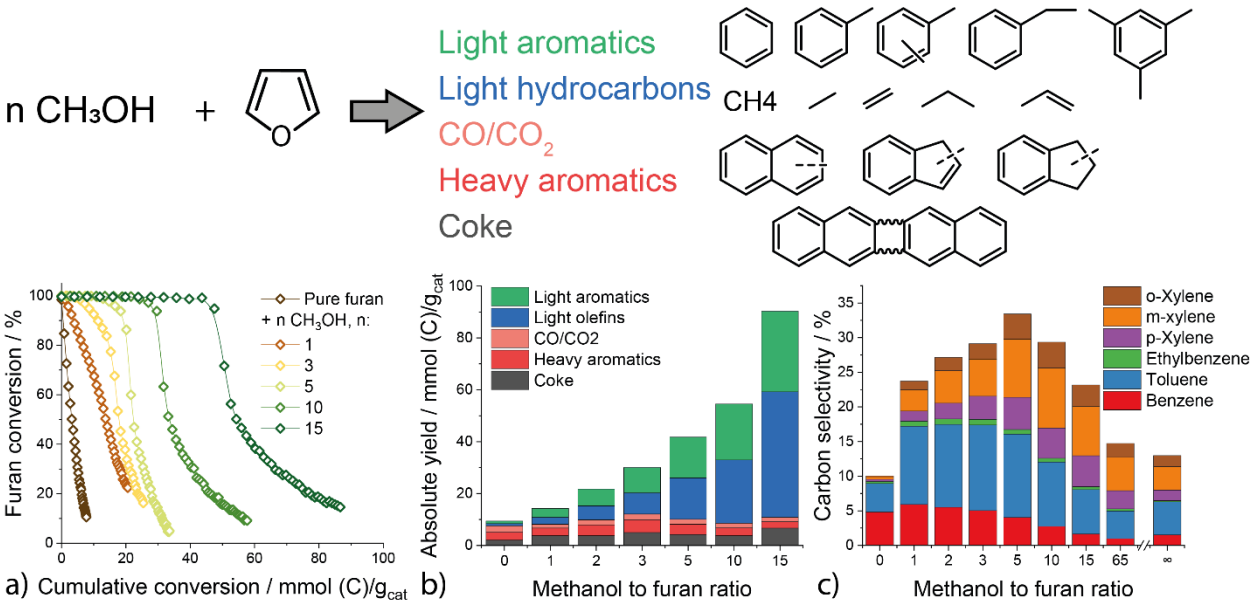

Figure 1. Summary of the catalytic results of furan co-feeding with n equivalents of methanol: a) conversion of furan as a function of total cumulative conversion computed as mmol C per gram of catalyst; b) absolute yields for the main groups of the reaction products; c) carbon selectivity

towards light aromatics. Conditions: reactor temperature 450 °C; p(Furan) 0.6 kPa; atmospheric pressure; carrier flow 100 mL/min He.

As shown in *Figure 1a*, the conversion of furan is initially close to 100% and rapidly decreases reaching 50% already after 20 min reaction due to coke deposition.[23,24] Addition of methanol to the feed substantially lowers the rate of deactivation and this effect becomes more pronounced when more methanol is added relative to furan. The total furan conversion increases from 4.5 mmol C/g_{cat}, when only furan is fed, to 10 mmol C/g_{cat} for a methanol/furan molar ratio of 15. The total cumulative carbon conversion with co-fed methanol increases by more than an order of magnitude to 50 mmol C/g_{cat}. Along with the improved lifetime, the addition of methanol significantly changes the product distribution. *Figures 1b,c* show that the (carbon-based) BTX selectivity improves with increasing methanol/furan ratio from 10% (pure furan) to 35% (methanol/furan – 5). At the same time, the fraction of the most valuable compounds in the BTX mixture, *i.e.* xylenes, increases from 8% to 64%. When the methanol/furan ratio is further increased, the BTX selectivity becomes lower and eventually approaches the value obtained with pure methanol feed. The higher concentration of xylenes and other methylated benzenes in the product mixture suggests that alkylation of benzene and toluene with methanol occurs. On the other hand, the formation of heavier bicyclic products such as indanes, indenes and naphthalenes is suppressed in the presence of methanol. This change in the product distribution can explain the observed slower deactivation rate, as polycyclic aromatics are considered to be coke precursors (See *Figure S1* for the complete distribution of the reaction products).[25–27] The product distribution significantly changes during the progress of the reaction as well (*Figures S2,3)*. At prolonged reaction times, a gradually increasing fraction of the catalyst becomes deactivated by coke deposits, resulting in a shortening of the effective contact time. Thus, the reaction time-on-stream profiles provide valuable information about the reaction intermediates.[28,29] The formation of

methylated furans, including 2-methylfuran and 2,5-dimethylfuran (2,5-dMF) was observed at a later stage of the reaction (*Figure S4*). As we previously showed, such methylated furans can undergo aromatization on zeolites by forming reaction intermediates with a lower C/H ratio upon initial deoxygenation (See *Figure S5*).[30] This results in a lower rate of coke formation and, therefore, a higher total BTX yield as compared to the conversion of unsubstituted furan. Besides, this is in line with the observed shift in deoxygenation pathway from dehydration/decarbonylation/decarboxylation to mainly dehydration (see *Table S2* for the distribution of oxygen-containing products), which was previously observed during conversion of methyl-substituted furans.[30]

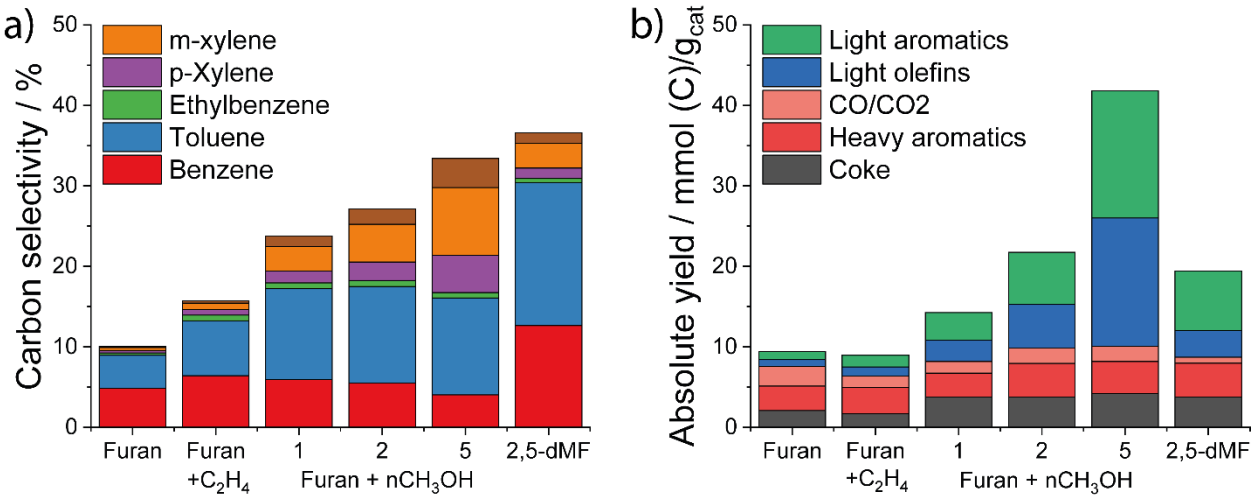

Figure 2. Overall (a) carbon selectivity and (b) absolute yields in pure furan aromatization reaction as compared to furan with co-feeding of 2 equivalents of methanol, furan with co-feeding ethylene and 2,5-dimethylfuran. Conditions: reactor temperature 450 °C; p(furan) 0.6 kPa; atmospheric pressure; carrier – 100 mL/min He.

In order to evaluate the importance of furan methylation and DA chemistry (pathways I, III in the *Scheme 1*) on the overall reaction performance we carried out additional catalytic experiments with (i) 2,5-dMF and (ii) furan with co-feeding ethylene and (iii) 2,5-dMF with co-feeding

ethylene. The carbon stoichiometry of these feeds was the same as for the co-reaction of furan with 2 equivalents of methanol (iii) (see *Figure 2* for the product distribution and yield).

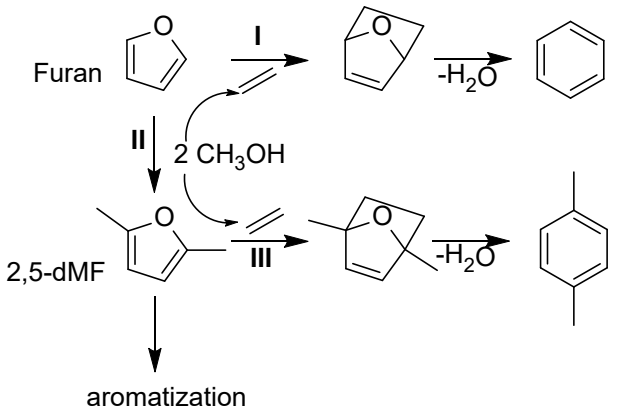

Scheme 1. Possible reaction pathways involving methanol in furan aromatization reaction: I. Diels-Alder pathway; II. methylation of furan followed by aromatization and III. Diels-Alder reaction with ethylene.

Strikingly, for the aromatization of furan in the presence of ethylene, we observe that both the absolute yield and the carbon selectivity to BTX were very close to values obtained for pure furan. A small increase in substituted aromatics production can be attributed to alkylation of the reaction products with ethylene.[31] A similar effect of ethylene co-feeding was previously described for the conversion of 2,5-dMF.[14] On the other hand, aromatization of pure 2,5-dMF led to a significantly higher aromatics selectivity (~35%) and absolute product yield. However, the distribution of aromatic products is different from that obtained when furan was co-fed with 2 equivalents of methanol. Both the absolute yield and the fraction of xylenes are higher when methanol is co-fed to furan. These findings imply that the positive influence of methanol cannot be solely attributed to either furan methylation followed by aromatization or to DA cycloaddition between furan and ethylene produced from methanol. Clearly, other reactions must be involved that lead to the strongly improved BTX selectivity and longer catalyst life when methanol is co-fed.

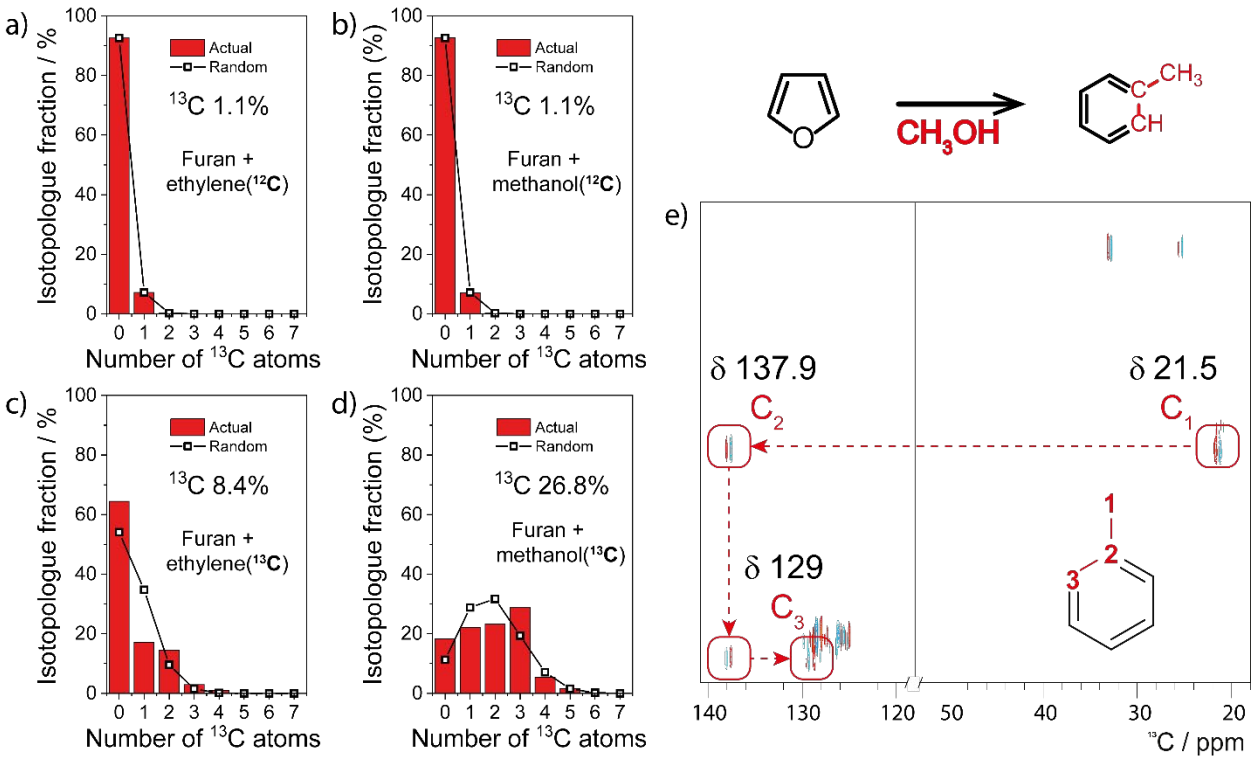

Figure 3. Isotope distribution in toluene obtained in a reaction of furan with addition of ethylene and methanol (a, b); ^{13}C labelled ethylene and methanol (c, d); e) INADEQUATE NMR spectrum of the reaction mixture obtained in presence of $^{13}CH_3OH$. Cross peaks corresponding to toluene product are labelled on the graph with respective chemical shifts.

Isotope labelling was applied to understand the role of co-fed methanol and ethylene in furan aromatization. Furan was co-fed with either ^{13}C-labeled ethylene $H_2{}^{13}C={}^{13}CH_2$ or ^{13}C-labeled methanol $^{13}CH_3OH$. The liquid reaction products collected in a LN_2 trap were analyzed by GC-MS and NMR. GC-MS analysis reveals that the ^{13}C atoms from ethylene and methanol are included in the reaction products. *Figure 3* shows MS spectra of toluene obtained after the reaction of furan with labelled ethylene and methanol. The initial ^{13}C content in the feed was 30% which corresponds to ethylene/furan molar ratio of 1 and methanol/furan molar ratio of 2. After the reaction of furan with ^{13}C-ethylene the ^{13}C content of toluene was 8.4%, and after the reaction of

furan with ^{13}C-methanol – 26.8%. The ^{13}C content of other aromatic products, produced in co-feeding experiments, was similar to these values (MS spectra of benzene, xylenes and naphthalenes are shown by *Figures S6 and S7;* ^{1}H and ^{13}C NMR spectrum can be found in *Figures S8-S11*). Since the ^{13}C contents of the reaction mixture and obtained aromatic products are the same, we can conclude that, co-aromatization between furan and methanol occurs. A more detailed analysis of the GC-MS data shows that the distribution of ^{13}C labels in toluene is not random (*Figure 3d*). The fraction of toluene molecules containing four unlabeled atoms is significantly higher than the expected value and this difference from a random distribution is also observed for the other aromatic molecules. In contrast to methanol case, ethylene incorporation into the reaction products is limited. For aromatics we observe a strong tendency to either remain unlabeled or to contain two ^{13}C atoms.

Due to the higher amount of ^{13}C, we could study the connectivity of ^{13}C atoms in the reaction products of furan – methanol co-aromatization, using ^{13}C-^{13}C homonuclear correlation NMR spectroscopy (*INADEQUATE*, see *Figure 3e*). Apart from a large number of ^{13}C-^{13}C bonds in the aromatic region of the *INADEQUATE* spectra, we found that in toluene the ^{13}C labels can form three ^{13}C chains starting from the aliphatic methyl group of the molecule (C_1 – C_3 in *Figure 3e*). This result is in accord with the GC-MS, emphasizing that the original four-carbon ^{12}C furan skeleton could remain intact during co-aromatization.

As described above, the addition of methanol to the feed lowers the rate of catalyst deactivation and is therefore expected to affect the structure of intra-zeolitic coke deposits. TG analysis of spent zeolite samples (*Figure S12)* shows a small shift to lower temperature (~10 °C) of the main combustion peak for samples obtained by furan co-aromatization with methanol in comparison to the sample obtained during furan aromatization and furan co-aromatization with ethylene. A higher

proton content of the coke species is a reasonable explanation for the more facile combustion.[26] By periodically burning the formed coke species in oxygen, we established that the catalyst could be regenerated at least 4 times without obvious changes in activity and selectivity (See *Figure S13*).

To establish the relation between the structure of carbon deposits and the composition of reactant mixture the catalyst samples after the reaction in pure furan and in mixtures of furan with ^{13}C-methanol/^{13}C-ethylene were studied by MAS NMR spectroscopy. The $^{13}C\{^{1}H\}$ cross-polarization (CP) and ^{13}C direct excitation (DE) NMR spectra are presented in *Figure 4a* and *Figure S14*, respectively. The sample exposed to pure furan exhibits a single broad signal at 130 ppm, corresponding to sp^2 carbon, assigned to intra-zeolite polyaromatic species.[32,33] Addition of labelled ethylene or methanol led to a new sharp signal at 20 ppm, attributed to aliphatic sp^3 carbon species.[34] Another signal at about 50 ppm was observed for samples obtained in furan/methanol and it can be assigned to methoxy groups.[35] The ^{13}C DE spectra shown in *Figures S14(b,c)* provide quantitative information about these intra-zeolite species. When ^{13}C-ethylene was co-fed with furan, we observed an 8-fold increase in the total ^{13}C intensity of coke as compared to the experiment with pure furan. This implies that surface carbon contains about 8% of ^{13}C atoms (natural abundance of ^{13}C is 1.1%). It should be noted that a similar ^{13}C content (~10%) was observed in liquid reaction products by GC-MS. Besides, the relative intensity of the aliphatic signal at 20 ppm for the reaction with ^{13}C-ethylene case is higher than for ^{12}C-ethylene, suggesting that ethylene preferentially impacts the aliphatic fraction of coke. Stronger effect was observed when furan was reacted with methanol. The total intensity of NMR signal was approximately 20 times higher (^{13}C fraction of ~20%), while the increase in aliphatic fraction was significantly more pronounced than for the ethylene case. It should be noted that the total coke content of the spent

catalysts was similar (*Figure S12*), confirming that the increase in NMR signals is only related to the isotope enrichment of coke.

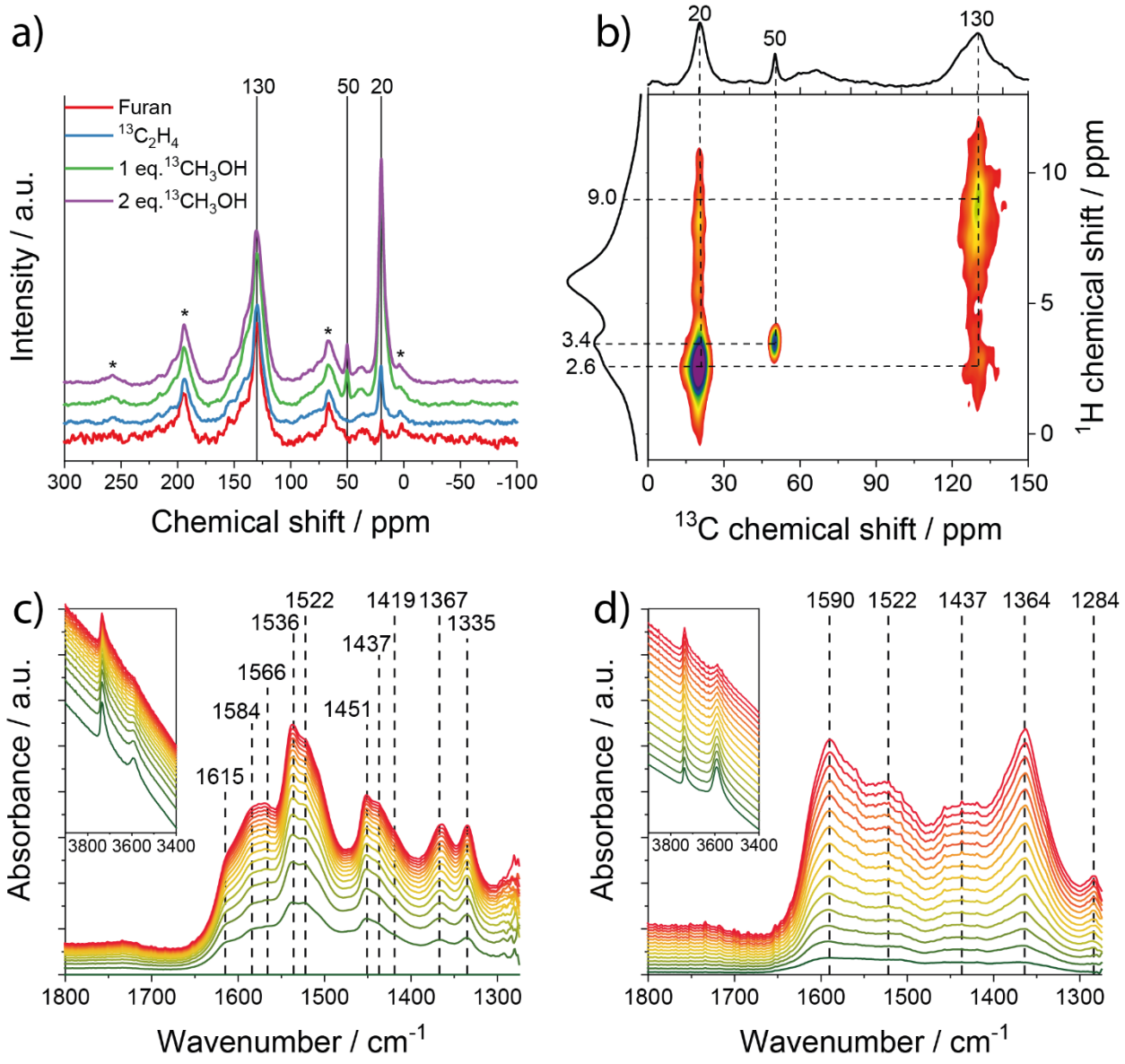

Figure 4. Formation of coke species in zeolite: a) ^{1}H-^{13}C CP MAS NMR of the samples obtained after the aromatization reaction of pure furan, furan-methanol and furan-ethylene mixtures; b) ^{1}H-^{13}C{^{1}H} HETCOR MAS NMR 2D spectrum of zeolite catalysts after furan aromatization reaction with co-feeding of ^{13}C methanol; IR spectra of 1800–1250 cm^{-1} region recorded under incremental dosing of b) furan c) a mixture of methanol and furan (2:1).

The ^{1}H-$^{13}C\{^{1}H\}$ heteronuclear correlation (HETCOR) MAS NMR experiments provide additional insights into the structure of retained species. The 2D spectrum shown in *Figure 4b* reveals complexity of the signal around 130 ppm. This might be attributed to different polyaromatic species interacting with Brønsted acid sites of zeolite. The data show a clear correlation between the aliphatic (20 ppm) and the aromatic (130 ppm) region, which suggests that aliphatic species are present as substituents in the aromatic molecules. We also followed the formation of intra-zeolite species with *in situ* IR spectroscopy (*Figure 4c,d* IR spectra of 1800–1250 cm^{-1} region, complete spectra in the *Supporting information*, *Figure S15*). For this purpose, a catalyst sample was exposed at 450 °C to either pure furan vapor or a vapor containing methanol and furan in a 2:1 molar ratio. The concentration of reactants in the cell was incrementally increased to 150 μmol C per Brønsted acid site (*Figure S15,* peak assignment summarized in *Table S3).* In both experiments, the dosing procedure led to a gradual disappearance of the bridging hydroxyl IR features at 3610 cm^{-1}, assigned to Brønsted acid sites.[36] Perturbed hydroxyls and water produced during decomposition of furan and methanol give rise to a broad band extending in the 3500–2000 cm^{-1} range (*Figure S15*). In the experiment with methanol, the disappearance of the unperturbed ν(OH) is much slower than in the experiment with pure furan. The formation of intra-zeolite hydrocarbon species is evident from the formation of bands at lower frequencies. These IR bands are very different for the two experiments. During the reaction with pure furan, bands assignable to fused polyaromatics develop. The band at 1610 cm^{-1} evidences formation of highly unsaturated polyaromatic deposits.[37] Less condensed polycyclic species give rise to bands at 1540–1520 cm^{-1}. The bands at 1350–1450 cm^{-1} are due to δ(CH) of unsaturated species.[37,38] When methanol is co-fed, two new bands are observed at 1590 cm^{-1} and 1364 cm^{-1}, corresponding to ν(CC) and δ(CH) vibrations of poly-methylated benzenes.[39] These results suggest that the intra-

zeolite species formed during co-aromatization of furan with methanol include a substantial amount of highly alkylated aromatic species in contrast to the exclusively sp^2 polyaromatics formed in pure furan. Based on these results we suggest that the alkyl termination makes it more difficult for the initial coke precursors to fuse into larger polyaromatic species, resulting in the decreased deactivation rate.

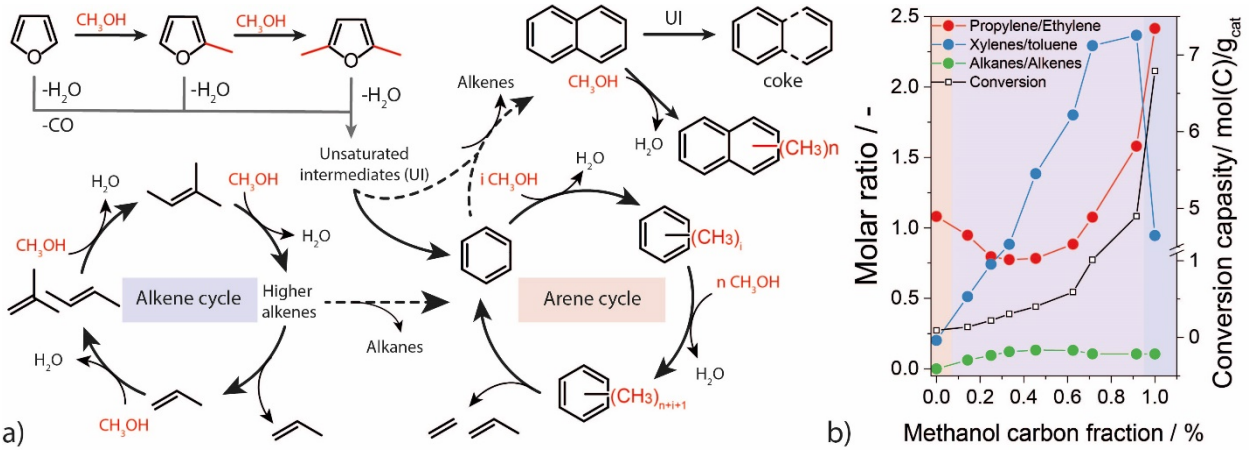

Figure 5. Proposed reaction pathways of furan conversion in presence of methanol on HZSM-5 zeolites including deoxygenation of furanics (grey line), alkylation (solid line) and transfer-dehydrogenation (dashed line) (a) and the main products molar carbon ratios as compared to cumulative carbon conversion per gram of catalyst in furan, furan-methanol mixtures and methanol (b).

Based on the presented data we put forward a mechanism for the co-aromatization of furanics with methanol (*Figure 5*). We propose that this reaction shares similarities with the Dual-Cycle hydrocarbon pool mechanism established for methanol-to-hydrocarbons (MTH) process. In this mechanism, a pool of hydrocarbon species including aromatics (arene cycle) and alkenes (alkene cycle) is responsible for the formation of hydrocarbon products.[40] In case of co-aromatization with methanol, furanic compounds undergo deoxygenation through either dehydration or decarbonylation to form highly proton-deficient intermediates.[30] Because of their low H/C ratio,

these intermediates are directly involved into the aromatic cycle. As indicated by MS and NMR data, methanol and furan undergo co-aromatization when co-fed and these processes are not separated mechanistically. An evident increase in the propylene/ethylene ratio and decrease in the alkane/alkene ratio with increasing methanol concentration, evidence that the reaction mechanism shifts from the predominant aromatic cycle to the alkene cycle upon increasing the concentration of methanol in the feed. Other important effects, resulting from methanol addition, are methylation of furan, methylation of aromatics in the arene cycle and methylation of heavier aromatics. Methylation of light aromatics explains the higher selectivity to xylenes. While methylation of polycyclic aromatics suppresses poly-condensation reactions and, in this way, lowers the coke formation rate.

Conclusions

In summary, this work demonstrates a potential of the methanol co-feeding concept to improve the catalytic performance of zeolite catalysts in aromatization of biomass-derived compounds. Based on a combination of catalytic, isotope labelling and spectroscopy data, we put forward a mechanistic proposal for the co-aromatization of furan with methanol. In this proposal furan aromatization over zeolites follows a hydrocarbon pool mechanism, previously observed for the MTH processes. Given that both furanics and methanol are potential carbon sources in the future carbon-neutral chemical industry, the co-feeding concept presents a promising way for the sustainable production of aromatics.

SUPPORTING INFORMATION

Physico-chemical properties of the catalysts, detailed catalytic activity data and product distribution, isotope distribution for labelling experiments, catalyst deactivation and coke characterization data.

CONFLICTS OF INTERESTS

There are no conflicts to declare.

ACKNOWLEDGMENT

This work was supported by the Netherlands Center for Multiscale Catalytic Energy Conversion (MCEC), an NWO Gravitation programme funded by the Ministry of Education, Culture and Science of the government of the Netherlands.

REFERENCES

(1) Sheldon, R. A. Green and Sustainable Manufacture of Chemicals from Biomass: State of the Art. *Green Chem.* **2014**, *16*, 950–963. https://doi.org/10.1039/C3GC41935E.

(2) Gallezot, P. Conversion of Biomass to Selected Chemical Products. *Chem. Soc. Rev.* **2012**, *41*, 1538–1558. https://doi.org/10.1039/C1CS15147A.

(3) Corma, A.; De La Torre, O.; Renz, M.; Villandier, N. Production of High-Quality Diesel from Biomass Waste Products. *Angew. Chemie - Int. Ed.* **2011**, *50*, 2375–2378. https://doi.org/10.1002/anie.201007508.

(4) Huber, G. W.; Corma, A. Synergies between Bio- and Oil Refineries for the Production of Fuels from Biomass. *Angew. Chemie - Int. Ed.* **2007**, *46*, 7184–7201. https://doi.org/10.1002/anie.200604504.

(5) Cheng, Y. T.; Huber, G. W. Chemistry of Furan Conversion into Aromatics and Olefins over HZSM-5: A Model Biomass Conversion Reaction. *ACS Catal.* **2011**, *1*, 611–628. https://doi.org/10.1021/cs200103j.

(6) Baerlocher, C.; McCusker, L. B.; Olson, D. H. Atlas of Zeolite Framework Types. In *Atlas of Zeolite Framework Types*; Elsevier: Amsterdam, 2007. https://doi.org/10.1016/B978-044453064-6/50228-0.

(7) Jae, J.; Tompsett, G. A.; Foster, A. J.; Hammond, K. D.; Auerbach, S. M.; Lobo, R. F.; Huber, G. W. Investigation into the Shape Selectivity of Zeolite Catalysts for Biomass Conversion. *J. Catal.* **2011**, *279*, 257–268. https://doi.org/10.1016/j.jcat.2011.01.019.

(8) Liu, C.; Wang, H.; Karim, A. M.; Sun, J.; Wang, Y. Catalytic Fast Pyrolysis of Lignocellulosic Biomass. *Chem. Soc. Rev.* **2014**, *43*, 7594–7623. https://doi.org/10.1039/C3CS60414D.

(9) Corma, A.; Huber, G. W.; Sauvanaud, L.; O'Connor, P. Processing Biomass-Derived Oxygenates in the Oil Refinery: Catalytic Cracking (FCC) Reaction Pathways and Role of Catalyst. *J. Catal.* **2007**, *247*, 307–327. https://doi.org/10.1016/j.jcat.2007.01.023.

(10) Venderbosch, R. H. A Critical View on Catalytic Pyrolysis of Biomass. *ChemSusChem* **2015**, *8*, 1306–1316. https://doi.org/10.1002/cssc.201500115.

(11) Cheng, Y.-T.; Huber, G. W. Production of Targeted Aromatics by Using Diels–Alder Classes of Reactions with Furans and Olefins over ZSM-5. *Green Chem.* **2012**, *14*, 3114–3125. https://doi.org/10.1039/c2gc35767d.

(12) Cheng, Y.-T.; Jae, J.; Shi, J.; Fan, W.; Huber, G. W. Production of Renewable Aromatic Compounds by Catalytic Fast Pyrolysis of Lignocellulosic Biomass with Bifunctional Ga/ZSM-5 Catalysts. *Angew. Chemie Int. Ed.* **2012**, *51*, 1387–1390. https://doi.org/10.1002/anie.201107390.

(13) Cheng, Y. T.; Wang, Z.; Gilbert, C. J.; Fan, W.; Huber, G. W. Production of P-Xylene from Biomass by Catalytic Fast Pyrolysis Using ZSM-5 Catalysts with Reduced Pore Openings. *Angew. Chemie - Int. Ed.* **2012**, *51*, 11097–11100. https://doi.org/10.1002/anie.201205230.

(14) Uslamin, E. A.; Luna-Murillo, B.; Kosinov, N.; Bruijnincx, P. C. A.; Pidko, E. A.; Weckhuysen, B. M.; Hensen, E. J. M. Gallium-Promoted HZSM-5 Zeolites as Efficient Catalysts for the Aromatization of Biomass-Derived Furans. *Chem. Eng. Sci.* **2019**, *198*,

305–316. https://doi.org/10.1016/j.ces.2018.09.023.

(15) Qi, X.; Fan, W. Selective Production of Aromatics by Catalytic Fast Pyrolysis of Furan with In Situ Dehydrogenation of Propane. *ACS Catal.* **2019**, 2626–2632. https://doi.org/10.1021/acscatal.8b04859.

(16) Zheng, A.; Zhao, Z.; Chang, S.; Huang, Z.; Zhao, K.; Wu, H.; Wang, X.; He, F.; Li, H. Maximum Synergistic Effect in the Coupling Conversion of Bio-Derived Furans and Methanol over ZSM-5 for Enhancing Aromatic Production. *Green Chem.* **2014**, *16*, 2580–2586. https://doi.org/10.1039/c3gc42251h.

(17) Wang, C.; Si, Z.; Wu, X.; Lv, W.; Bi, K.; Zhang, X.; Chen, L.; Xu, Y.; Zhang, Q.; Ma, L. Mechanism Study of Aromatics Production from Furans with Methanol over Zeolite Catalysts. *J. Anal. Appl. Pyrolysis* **2019**, *139*, 87–95. https://doi.org/10.1016/j.jaap.2019.01.013.

(18) Goeppert, A.; Czaun, M.; Jones, J.-P.; Surya Prakash, G. K.; Olah, G. A. Recycling of Carbon Dioxide to Methanol and Derived Products – Closing the Loop. *Chem. Soc. Rev.* **2014**, *43*, 7995–8048. https://doi.org/10.1039/C4CS00122B.

(19) Olah, G. A.; Goeppert, A.; Prakash, G. K. S. Beyond Oil and Gas: The Methanol Economy. *Angew. Chemie - Int. Ed.* **2005**, *44*, 2636–2639. https://doi.org/10.1002/9783527627806.

(20) Olah, G. A. Towards Oil Independence Through Renewable Methanol Chemistry. *Angew. Chemie Int. Ed.* **2013**, *52*, 104–107. https://doi.org/10.1002/anie.201204995.

(21) Datka, J. Acidic Properties of Supported Niobium Oxide Catalysts: An Infrared

Spectroscopy Investigation. *J. Catal.* **1992**, *135*, 186–199. https://doi.org/10.1016/0021-9517(92)90279-Q.

(22) Emeis, C. A. Determination of Integrated Molar Extinction Coefficients for Infrared Absorption Bands of Pyridine Adsorbed on Solid Acid Catalysts. *J. Catal.* **1993**, *141*, 347–354. https://doi.org/10.1006/jcat.1993.1145.

(23) Rojo-Gama, D.; Mentel, L.; Kalantzopoulos, G. N.; Pappas, D. K.; Dovgaliuk, I.; Olsbye, U.; Lillerud, K. P.; Beato, P.; Lundegaard, L. F.; Wragg, D. S.; Svelle, S. Deactivation of Zeolite Catalyst H-ZSM-5 during Conversion of Methanol to Gasoline: Operando Time- and Space-Resolved X-Ray Diffraction. *J. Phys. Chem. Lett.* **2018**, *9*, 1324–1328. https://doi.org/10.1021/acs.jpclett.8b00094.

(24) Mores, D.; Stavitski, E.; Kox, M. H. F.; Kornatowski, J.; Olsbye, U.; Weckhuysen, B. M. Space- And Time-Resolved in-Situ Spectroscopy on the Coke Formation in Molecular Sieves: Methanol-to-Olefin Conversion over H-ZSM-5 and H-SAPO-34. *Chem. - A Eur. J.* **2008**, *14*, 11320–11327. https://doi.org/10.1002/chem.200801293.

(25) Rojo-Gama, D.; Nielsen, M.; Wragg, D. S.; Dyballa, M.; Holzinger, J.; Falsig, H.; Lundegaard, L. F.; Beato, P.; Brogaard, R. Y.; Lillerud, K. P.; Olsbye, U.; Svelle, S. A Straightforward Descriptor for the Deactivation of Zeolite Catalyst H-ZSM-5. *ACS Catal.* **2017**, *7*, 8235–8246. https://doi.org/10.1021/acscatal.7b02193.

(26) Mores, D.; Kornatowski, J.; Olsbye, U.; Weckhuysen, B. M. Coke Formation during the Methanol-to-Olefin Conversion: In Situ Microspectroscopy on Individual H-ZSM-5 Crystals with Different Brønsted Acidity. *Chem. - A Eur. J.* **2011**, *17*, 2874–2884.

https://doi.org/10.1002/chem.201002624.

(27) Schmidt, J. E.; Poplawsky, J. D.; Mazumder, B.; Attila, Ö.; Fu, D.; de Winter, D. A. M.; Meirer, F.; Bare, S. R.; Weckhuysen, B. M. Coke Formation in a Zeolite Crystal During the Methanol-to-Hydrocarbons Reaction as Studied with Atom Probe Tomography. *Angew. Chemie - Int. Ed.* **2016**, *55*, 11173–11177. https://doi.org/10.1002/anie.201606099.

(28) Haw, J. F.; Marcus, D. M. Well-Defined (Supra)Molecular Structures in Zeolite Methanol-to-Olefin Catalysis. *Top. Catal.* **2005**, *34*, 41–48. https://doi.org/10.1007/s11244-005-3798-0.

(29) Schulz, H. "Coking" of Zeolites during Methanol Conversion: Basic Reactions of the MTO-, MTP- and MTG Processes. *Catal. Today* **2010**, *154*, 183–194. https://doi.org/10.1016/j.cattod.2010.05.012.

(30) Uslamin, E. A.; Kosinov, N. A.; Pidko, E. A.; Hensen, E. J. M. Catalytic Conversion of Furanic Compounds over Ga-Modified ZSM-5 Zeolites as a Route to Biomass-Derived Aromatics. *Green Chem.* **2018**, *20*, 3818–3827. https://doi.org/10.1039/C8GC01528G.

(31) Smirniotis, P. G.; Ruckenstein, E. Alkylation of Benzene or Toluene with MeOH or C2H4 over ZSM-5 or .Beta. Zeolite: Effect of the Zeolite Pore Openings and of the Hydrocarbons Involved on the Mechanism of Alkylation. *Ind. Eng. Chem. Res.* **1995**, *34*, 1517–1528. https://doi.org/10.1021/ie00044a002.

(32) Kosinov, N.; Wijpkema, A. S. G.; Uslamin, E.; Rohling, R.; Coumans, F. J. A. G.; Mezari, B.; Parastaev, A.; Poryvaev, A. S.; Fedin, M. V.; Pidko, E. A.; Hensen, E. J. M. Confined Carbon Mediating Dehydroaromatization of Methane over Mo/ZSM-5. *Angew. Chemie Int.*

Ed. **2018**, *57*, 1016–1020. https://doi.org/10.1002/anie.201711098.

(33) Du, S.; Gamliel, D. P.; Giotto, M. V.; Valla, J. A.; Bollas, G. M. Coke Formation of Model Compounds Relevant to Pyrolysis Bio-Oil over ZSM-5. *Appl. Catal. A Gen.* **2016**, *513*, 67–81. https://doi.org/10.1016/j.apcata.2015.12.022.

(34) Chowdhury, A. D.; Houben, K.; Whiting, G. T.; Mokhtar, M.; Asiri, A. M.; Al-Thabaiti, S. A.; Basahel, S. N.; Baldus, M.; Weckhuysen, B. M. Initial Carbon–Carbon Bond Formation during the Early Stages of the Methanol-to-Olefin Process Proven by Zeolite-Trapped Acetate and Methyl Acetate. *Angew. Chemie - Int. Ed.* **2016**, *55*, 15840–15845. https://doi.org/10.1002/anie.201608643.

(35) Ivanova, I. I.; Corma, A. Surface Species Formed and Their Reactivity during the Alkylation of Toluene by Methanol and Dimethyl Ether on Zeolites As Determined by in Situ 13 C MAS NMR. *J. Phys. Chem. B* **1997**, *101*, 547–551. https://doi.org/10.1021/jp961468k.

(36) Bordiga, S.; Lamberti, C.; Bonino, F.; Travert, A.; Thibault-Starzyk, F. Probing Zeolites by Vibrational Spectroscopies. *Chem. Soc. Rev.* **2015**, *44*, 7262–7341. https://doi.org/10.1039/C5CS00396B.

(37) Karge, H. G.; Nießen, W.; Bludau, H. In-Situ FTIR Measurements of Diffusion in Coking Zeolite Catalysts. *Appl. Catal. A Gen.* **1996**, *146*, 339–349. https://doi.org/10.1016/S0926-860X(96)00175-5.

(38) Vimont, A.; Marie, O.; Gilson, J. P.; Saussey, J.; Thibault-Starzyk, F.; Lavalley, J. C. In Situ Infrared Study of Hydroxyl Groups Poisoned by Coke Formation from Hydrocarbons

Conversion on H-Zeolites. In *Studies in Surface Science and Catalysis*; 1999; Vol. 126, pp 147–154. https://doi.org/10.1016/S0167-2991(99)80461-3.

(39) Saepurahman; Visur, M.; Olsbye, U.; Bjørgen, M.; Svelle, S. In Situ FT-IR Mechanistic Investigations of the Zeolite Catalyzed Methylation of Benzene with Methanol: H-ZSM-5 versus H-Beta. *Top. Catal.* **2011**, *54*, 1293–1301. https://doi.org/10.1007/s11244-011-9751-5.

(40) Martínez-Espín, J. S.; De Wispelaere, K.; Janssens, T. V. W.; Svelle, S.; Lillerud, K. P.; Beato, P.; Van Speybroeck, V.; Olsbye, U. Hydrogen Transfer versus Methylation: On the Genesis of Aromatics Formation in the Methanol-To-Hydrocarbons Reaction over H-ZSM-5. *ACS Catal.* **2017**, *7*, 5773–5780. https://doi.org/10.1021/acscatal.7b01643.